A Robust, Multi-length Scale, Machine Learning Potential for Ag-Au Bimetallic Alloys from Clusters to Bulk Materials

Christopher M. Andolina[1], Marta Bon[2,†], Daniele Passerone[2] and Wissam A. Saidi[1*]

[1] Department of Mechanical Engineering and Materials Science, University of Pittsburgh, Pittsburgh, PA 15216, USA

[2] Empa, Swiss Federal Laboratories for Materials Science and Technology, Electron Microscopy Center, Überlandstrasse 129, CH-8600 Dübendorf, Switzerland

[†] M.B. Current address, CRUK Beatson Research Institute, University of Scotland, Glasgow G61 1BD, United Kingdom

Table of Contents

Bulk Crystal Lattice Constant and Atomic Energy.

The lattice constant of the system and the cohesive energy (E_{coh}) are determined from the optimized crystal structure. For elemental Ag and Au systems, we computed the cohesive energy per atom using equation **1**,

$$E_{coh} = E_B - E_{atom} \quad (\mathbf{1})$$

where E_B is the bulk energy per atom and E_{atom} is the energy of the corresponding isolated atom. Thus, with this definition, a negative E_{coh} indicates that the system is thermodynamically stable.

General Elastic Moduli Equations.

In the DFT and the atomistic calculations, the elastic constants are calculated using strain-stress relationships by performing 12 distortions of the optimum lattice and then fully relaxing the atomic coordinates. The bulk moduli (e.g., bulk, shear, Young's moduli, and Poisson's ratios) are computed using the crystal lattice specific equations.[1-3]

$$K_H = \frac{K_V + K_R}{2}$$

$$G_H = \frac{G_V + G_R}{2}$$

$$E_H = \frac{9K_H G_H}{3K_H + G_H}$$

$$v = \frac{3K_H - 2G_H}{6K_H + 2G_H}$$

Cubic systems

$$K_{V,G} = \frac{C_{11} + 2C_{22}}{3}$$

$$G_V = \frac{3C_{44} + C_{11} - C_{12}}{5}$$

$$G_R = \frac{5C_{44}(C_{11} + C_{12})}{4C_{44} + 3(C_{11} - C_{12})}$$

Point Defects.

Physical crystal structures are far from perfect or defect-free. Therefore, theoretical models need to reproduce defect formation energies and atomic structures accurately. We have investigated a selected group of point defects to evaluate the robustness of the Ag-Au DNP potential. Namely, we determined the energies of mono-vacancies, $\mathrm{E_{vac}}$, along with their activation energies for diffusion. Also, we examined mono self- and dumbbell-interstitials. **Table S1** summarizes the formation energies. Overall, as seen from the table, DFT reproduces well the defects with low formation energies but somewhat overestimates those with higher formation energies, consistent with other systems such as Cu-Zr[4]. The DFT diffusion energy barrier $\mathrm{E_{vac,mig}}$ associated with the vacancy movement to an adjacent position within the lattice is in excellent agreement with the experimental value. DFT predicts that Ag has a smaller diffusion barrier than Au, consistent with the experiment (**Figure S1**). Also, as noted before in other fcc lattices[4], the DFT energy of the $\mathrm{Ag[100]_{db}}$ is found to be the lowest energy of the dumbbell series. Inspecting the results obtained using atomistic potentials, we see an excellent agreement between DNP and DFT with an absolute average difference between the values of 0.066, while both EAMs perform similarly and have an order of magnitude larger error.

Vacancies.

Vacancy defects are modeled by taking a bulk crystal model and randomly removing an atom. This model is then optimized, and the vacancy formation energy (Eq. **S2**)

$$\mathrm{E_{vac}} = \mathrm{E} - \mathrm{NE_B} \qquad (\mathbf{S2})$$

Where $\boldsymbol{E}$ is the total energy of the optimized system with the defect, and $\boldsymbol{N}$ is the number of atoms and EB the per-atom energy of the bulk. In the point defect calculations, we used superlattices with 2x2x2 unit cells.

Self Interstitials.

The interstitial formation energies E_f are computed similarly to the vacancy case. We examined interstitial defects located at unique symmetry points. For the octahedral (Oh) site, an adatom is inserted at the [½, ½, ½] position of the primitive unit cell. For a tetrahedral (Td) site, an atom is added to the [¼, ¼, ¼] position.

Dumbbells.

Dumbbell defects (also known as split defects) were created by removing an atom and replacing it with a pair of atoms placed such that the midway point between them sits at the old location of the atom. Depending on orientation, atoms were placed such that they were equidistant between the nearest neighbor (or interstitial site) along the dumbbell axis and the other dumbbell atom. For these fcc metals, three types of dumbbells were modeled with their axis parallel to the [100], [110], or [111] direction. We have verified that dumbbell defects retain their original orientation by visual inspection of the final structures after optimization.

Vacancy Mobility Energy.

The vacancy mobility energy was determined using the nudged elastic band method (NEB) calculations[5] utilizing LAMMPS[6] software. The vacancy path was mapped using 16 frames.

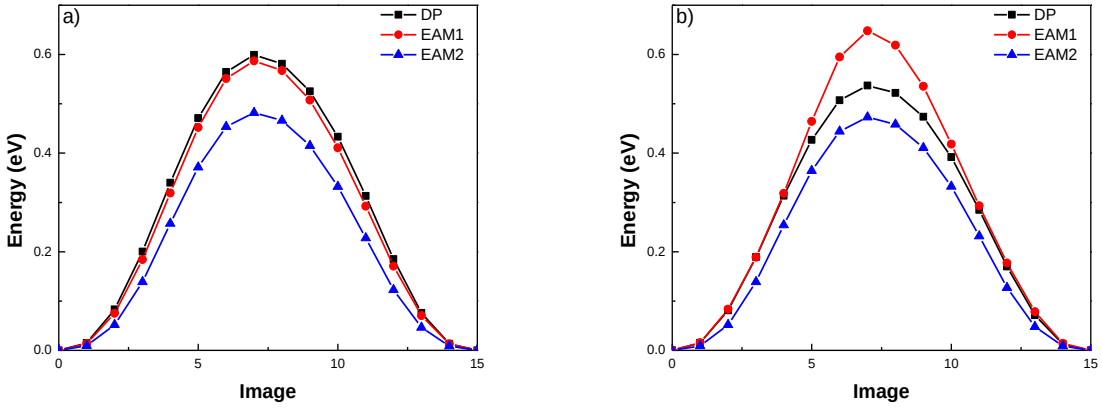

Figure S1. Sample Energy barrier for vacancy migration ($E_{vac,\ mig}$) via NEB DNP for (a) Ag and (b) Au. Lines added to guide the eye.

Table S1. Experimental and Computed Point Defect Energies for Ag and Au.

Point Defect Energy (eV)	EXP	DNP	EAM1[7]	EAM2[8]	DFT
Ag E_{vac}	1.1[64]	0.779	1.110	1.100	1.03
Ag $E_{vac,mig}$	0.66[64]	0.599	0.587	0.482	
Ag E_f (Oh)		2.373	3.260	3.030	2.38
Ag E_f (Td)		3.456	3.810	3.530	3.89
Ag E_f $[100]_{db}$		2.493	3.260	2.950	2.32
Ag E_f $[110]_{db}$		3.640	3.500	3.230	3.31
Ag E_f $[111]_{db}$		3.415	3.750	3.540	3.47
Au E_{vac}	1.0[64]	0.594	1.030	0.990	0.36
Au $E_{vac,mig}$	0.88[65]	0.537	0.648	0.473	
Au E_f (Oh)		2.323	2.610	2.830	2.34
Au E_f (Td)		3.889	2.710	3.120	4.74
Au E_f $[100]_{db}$		2.618	2.470	2.730	3.78
Au E_f $[110]_{db}$		2.285	2.580	2.900	2.36
Au E_f $[111]_{db}$		3.828	2.670	3.070	3.96

All energies are in eV. All DFT values in this table are calculated for this work.

Table S2. Comparison of Ag and Au Clusters 3D *versus* 2D structures (ΔEnergy, eV)

Cluster	DNP	EAM1[7]	EAM2[8]	DFT
Ag_6	0.18	0.00	0.00	0.24
Ag_7	-0.04	0.40	0.00	-0.39
Ag_8	-0.04	0.08	0.48	-0.58
Ag_9	-0.05	-0.32	0.17	-0.44
Au_6	0.809	1.289	0.000	0.97
Au_7	0.918	0.411	0.171	0.70
Au_8	1.197	0.603	0.000	0.67
Au_9	0.852	-0.619	-0.652	0.63

All DFT values in this table are calculated for this work.

Table S3. EAM, and DNP, DFT values other Ag and Au lattices.

Properties	DNP	EAM1[7]	EAM2[8]	DFT
Ag hcp a	2.93	2.87	2.89	2.95
Ag hcp c	4.81	4.71	4.75	4.79
Ag hcp E_0	-2.69	-2.85	-2.85	-2.83
Ag V_0	17.83	16.78	17.22	16.08
Ag bcc (Å)	3.30	3.23	5.94	3.30
Ag bcc E_0	-2.69	-2.81	-1.85	-2.75
Ag V_0	17.99	16.92	26.22	17.97
Ag diamond	6.21	6.08	3.28	6.71
Ag diamond E_0	-1.97	-1.91	-2.82	-2.33
Ag diamond V_0	29.98	28.12	17.67	29.36
Ag sc	2.76	2.69	2.70	2.70
Ag sc E_0	-2.37	-2.42	-2.45	-2.01
Ag V_0	20.963	19.56	19.68	19.68
Au hcp a	2.935	2.867	2.882	2.910
Au hcp c	5.000	4.712	4.736	4.889
Au hcp E_0	-3.180	-3.920	-3.929	-3.350
Au V_0	22.011	16.774	17.032	20.699
Au bcc	3.312	3.240	3.256	3.130
Au bcc E_0	-3.180	-3.874	-3.900	-3.190
Au V_0	14.905	17.014	17.255	18.132
Au diamond	6.201	5.951	5.797	6.381
Au diamond E_0	-2.642	-3.042	-2.935	-2.469
Au V_0	27.904	26.347	24.350	25.984
Au sc	2.751	2.688	2.678	2.750
Au sc E_0	-2.954	-3.464	-3.579	-2.634
Au V_0	20.829	19.420	19.208	20.797

All DFT calculations from this work. hcp (a and c), bcc, diamond, and sc lattice constants in Å, E_0 in eV/atom, and V_0 in $Å^3$.

Surface Energies.
The surface formation energy γs is computed using equation **3**.

$$\gamma s = (\mathrm{E_{slab}} - \mathrm{NE_B})/(2\mathrm{A}) \qquad (\mathbf{S3})$$

Here $\mathrm{E_{slab}}$ is the energy of the slab model and A is the surface area perpendicular to the slab direction, and N is the number of atoms in the slab. The factor of 2 is included to account for the two surfaces in the slab models.

Table S4. Surface Energies γ_s in mJ/m^2 for Ag slabs.

Surface Termination	γ_s Ag			
	DNP	EAM1[7]	EAM2[8]	DFT[9]
100	821	702	977	820
110	871	764	1084	870
111	695	617	905	760
210	940	1157	1143	900
211	843	1105	1061	879
221	829	1084	1043	820
310	925	1161	1125	890
311	877	1129	1094	860
320	931	1165	1141	890
321	880	1142	1111	860
322	809	1057	1015	770
331	857	1117	1077	850
332	801	1035	1002	790

All DFT values are taken from the MPDB.

Table S5. Surface Energies γ_s in mJ/m^2 for Au slabs.

Surface Termination	γ_s Au			
	DNP	EAM1[7]	EAM2[8]	DFT[9]
100	821	702	977	820
110	871	764	1084	870
111	695	617	905	760
210	940	1157	1143	900
211	843	1105	1061	879
221	829	1084	1043	820
310	925	1161	1125	890
311	877	1129	1094	860
320	931	1165	1141	890
321	880	1142	1111	860
322	809	1057	1015	770
331	857	1117	1077	850
332	801	1035	1002	790

All DFT values are taken from the MPDB.

Planar Defects Energies.
Similar to the terminated surface energy, we validated our DNP on various planar defects and compared our results to those listed in the MPDB.

Table S6. Ag Planar Defects surfaces energies in mJ/m^2.

Sigma	Defect Plane	Rotation Plane	Rotation	γ_s Ag			
				DNP	EAM1[7]	EAM2[8]	DFT
3	$1\bar{1}2$	110	180.0	586	615	553	540
3	$1\bar{1}0$	111	109.47	362	436	408	430
3	111	111	60.00	8.12	-19	24	70
5	$0\bar{1}3$	100	53.13	491	646	595	550
5	$0\bar{2}1$	100	36.87	531	711	671	590
5	100	100	36.87	407	497	458	420
7	111	111	36.87	183	222	205	210
7	$3\bar{2}1$	111	38.21	515	675	624	540
9	110	110	38.94	458	609	580	510
9	$2\bar{2}1$	110	38.94	677	892	814	710

All DFT calculations from this work.

Table S7. Au Planar Defects surfaces energies in mJ/m^2.

Sigma	Defect Plane	Rotation Plane	Rotation	γ_s Au			
				DNP	EAM1[7]	EAM2[8]	DFT
3	$1\bar{1}2$	110	180.0	603	629	543	460
3	$1\bar{1}0$	111	109.47	254	437	409	340
3	111	111	60.00	74	35	35	30
5	$0\bar{1}3$	100	53.13	499	756	620	450
5	$0\bar{2}1$	100	36.87	497	775	663	520
5	100	100	36.87	351	502	456	320
7	111	111	36.87	404	711	622	440
7	$3\bar{2}1$	111	38.21	181	300	206	170
9	110	110	38.94	412	635	571	390
9	$2\bar{2}1$	110	38.94	613	979	818	610

All DFT calculations from this work.

Comparison of Potentials.
Comparing all properties of bulk Ag reveals similar accuracy compared to the DFT calculations for all three models DNP, EAM1, and EAM2, with absolute $\%E_{DIF}$ of 14.5 and 30.9 and 33.5, respectively. Further, the average total difference of DFT values from the selected experimental values is 29.9, which indicates that DFT can describe experimental values relatively well. For the Au validation properties, the two EAM atomistic force-fields reproduce the DFT with a similar accuracy of 31.2 and 31.9, nearly a factor of 2 larger than that of the DNP model (13.6). The difference between the experimental and DFT values is more prominent than what we observed for the Ag data with a value of 43.9, which is likely to influence heavy atom effects of Au such as spin-orbit coupling and relativistic effects.

Comparison of Core-Shell NP Growth via DNP and DFT.
We simulated Au growth on a Ag NP using DFT and compared it with our DNP results to find good agreement (**Figure S2**). As DFT calculations have a much greater computation cost, we limited our DFT comparisons to time points 0, 50,100, and 200 ns. We observe less than 2.2 % error or 0.8 eV (50 ns time point) difference between the DNP and DFT Au@Ag NP growth for all time frames compared.

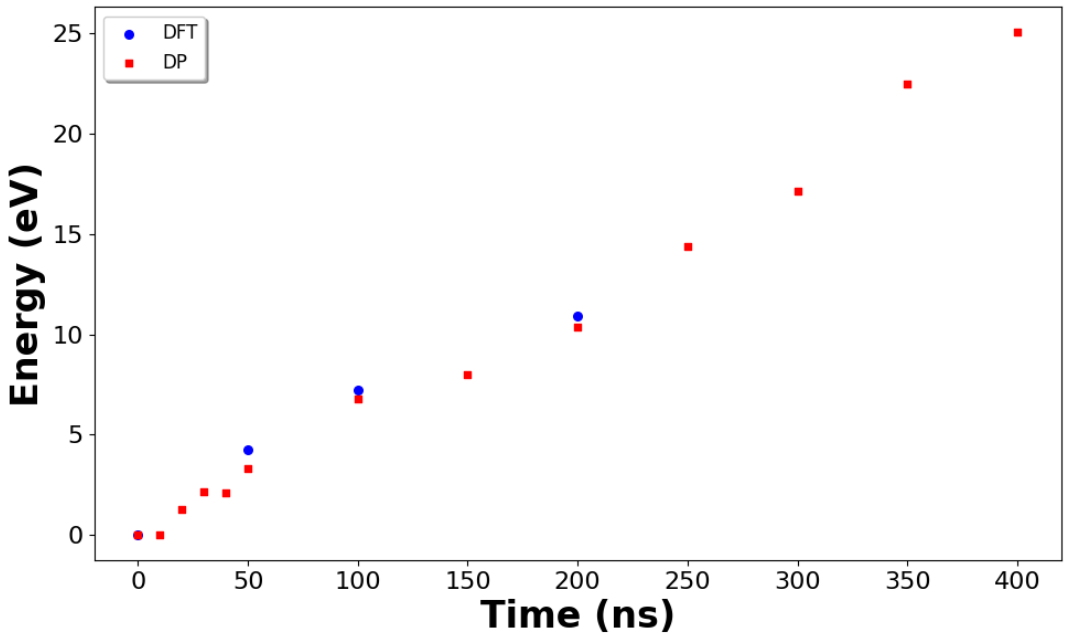

Figure S2. Comparison of DNP and DFT showing the difference in energies during Au@Ag NP growth various timepoints.

References.

1. Hill, R., The Elastic Behaviour of a Crystalline Aggregate. *Proc. Phys. Soc., A* **1952**, *65*, 349-354.
2. Reuss, A., Berechnung Der Fließgrenze Von Mischkristallen Auf Grund Der Plastizitätsbedingung Für Einkristalle. *Z. Angew. Math. Mech.* **1929**, *9*, 49-58.
3. Voigt, W., *Lehrbuch Der Kristallphysik*; Teubner Leipzig, 1928; Vol. 962.
4. Andolina, C. M.; Williamson, P.; Saidi, W. A., Optimization and Validation of a Deep Learning Cuzr Atomistic Potential: Robust Applications for Crystalline and Amorphous Phases with near-Dft Accuracy. *J Chem. Phys.* **2020**, *152*, 154701.
5. Henkelman, G.; Uberuaga, B. P.; Jónsson, H., A Climbing Image Nudged Elastic Band Method for Finding Saddle Points and Minimum Energy Paths. *J. Chem. Phys.* **2000**, *113*, 9901-9904.
6. Plimpton, S., Fast Parallel Algorithms for Short-Range Molecular Dynamics. *J. Comput. Phys.* **1995**, *117*, 1-19.
7. Foiles, S. M.; Baskes, M. I.; Daw, M. S., Embedded-Atom-Method Functions for the Fcc Metals Cu, Ag, Au, Ni, Pd, Pt, and Their Alloys. *Phys. Rev. B* **1986**, *33*, 7983-7991.
8. Zhou, X. W.; Johnson, R. A.; Wadley, H. N. G., Misfit-Energy-Increasing Dislocations in Vapor-Deposited Cofe/Nife Multilayers. *Phys. Rev. B* **2004**, *69*, 144113.
9. Jain, A., et al., Commentary: The Materials Project: A Materials Genome Approach to Accelerating Materials Innovation. *APL Mater.* **2013**, *1*, 011002.